Wireless Hybrid Vehicle Three-Phase Motor Diagnosis Using Z-Freq Due to Unbalance Fault

N.A. Ngatiman[1*], M.N.B. Othman[1,2], M.Z. Nuawi[2]

[1]Faculty of Mechanical and Manufacturing Engineering Technology,
 Universiti Teknikal Malaysia Melaka, Durian Tunggal, Melaka, MALAYSIA

[2]Faculty of Engineering and Built Environment,
 Universiti Kebangsaan Malaysia, Bangi, Selangor, MALAYSIA

*Corresponding Author

Abstract: Online diagnostics of three phase motor rotor faults of hybrid vehicle can be identified using a method called machine learning. Unfortunately, there is still a constraint in achieving a high success rate because a huge volume of training data is required. These faults were represented on its frequency content throughout the Fast Fourier Transform (FFT) algorithm to observe data acquired from multi-signal sensors. At that point, these failure-induced faults studies were improved using an enhanced statistical frequency-based analysis named Z-freq to optimize the study. This analysis is an investigation of the frequency domain of data acquired from the turbine blade after it runs under a specific condition. During the experiment, the faults were simulated by equipment with all those four conditions including normal mode. The failure induced by fault signals from static, coupled and dynamic were measured using high sensitivity, space-saving and a durable piezo-based sensor called a wireless accelerometer. The obtained result and analysis showed a significant pattern in the coefficient value and distribution of Z-freq data scattered for all flaws. Finally, the simulation and experimental output were verified and validated in a series of performance metrics tests using accuracy, sensitivity, and specificity for prediction purposes. This outcome has a great prospect to diagnose and monitor hybrid electric motor wirelessly.

Keywords: Statistical signal analysis, rotor unbalance, rotor diagnostic, wireless monitoring

1. Introduction

Hybrid Electric Vehicles (HEVs) have become popular these days as they consist of electric drive components and Internal Combustion Engines (ICE). The increase and instability of fuel prices today are among the driving factors of having more efficient and fuel-saving vehicles. Lebanon, for example, encourages the sale of fuel-efficient cars by doubling fuel taxes. These policies and lower fuel consumption are the main factors in increasing the market share of HEVs from 9.25% to 9.59%. [1] HEVs also play an essential role when concerned with climate change. Less carbon monoxide and carbon dioxide released by vehicles would help reduce the greenhouse effect. Unlike electric vehicles (EVs) that need infrastructure to recharge their batteries, HEVs batteries are charged from ICE and kinetic energy when the car moves. There are three categories of HEVs: parallel, series HEVs, and power-splits HEVs. These are categories concerning the mechanical connection and the vehicle's power flow. Parallel HEVs is classified when ICE and electric motor can simultaneously drive the car. Series HEVs are classified when the first power source is the electric motor powered by a battery and ICE charges the battery.

Meanwhile, Power-splits HVEs, also known as series-parallel HEVs is classified when there is isolation between ICE and the vehicle powertrain. From all three categories, the main components that exist in all the categories are the

engine, electric motor, and powertrain [2]. Proper maintenance of HEVs is essential as it is a complicated system with mechanical and electrical drives on one system. One may need, for example, to monitor an electric motor so that it can last longer and not affect another component connected to it. There are several issues with electric motors on vibration: motor frame, rotor imbalance, motor bearing and stator winding. In focusing on rotor imbalance, N. Wang and Jiang (2018) said the main problem is miss alignment which may cause a strong vibration toward the system, which is also agreed by P. Wang et al. (2022), that mention that bearing misalignment significantly influences dynamic characteristics in the low-speed range, while Cao et al. (2018) mention that the unbalanced rotor is due to angular speed fluctuation however, Jian et al. (2022) claimed that the rotor unbalances expected to load changes and rust.

Good monitoring would help reduce undesired problems due to electric motors in HEVs. For example, a self-sensing piezoelectric actuator was used by Ambur and Rinderknecht (2018) to detect the unbalance on rotor. By having images or data from the field, the health of individual machines could be lengthened. Several methods are currently used to monitor the health of individual devices, such as vibration, temperature, and an acoustic signal from the operating machine. (Mongia et al. 2022) Failure to detect incoming faults would bring catastrophic failure of the equipment, more extended downtime, and higher repair costs.

Thus, having fault data is essential to further study and categorize the problems that may affect the unbalanced rotor. Fault data can also be created in the fault simulator machine's test rig machine. N. Wang and Jiang (2018) studied the response of a dual rotor system with an unbalanced-misalignment coupling fault using the Runge Kuta method. The fault was done by adjusting the height and quantity of gaskets and installing a screw on the disk on the inner rotor. While the Gaussian-SVM method was by Lan et al. (2023) to improve sensitivity diagnosis of rotor unbalance faults. Nevertheless, there are still analytical methods used as prognostic in rotor bearing condition maintenance strategy. [10]

The most common analysis methods in machine monitoring are peak, RMS, crest factor, and kurtosis. Ahmad et al. (2018) developed tool wear monitoring via I-kaz^{TM} statistical signal analysis. The researcher able to monitor tool wear efficiently with 1.8 to 15.9 errors. Frequency-based domain, Z-freq was developed by Ngatiman et al. (2018) to monitor gasoline engine misfire conditions on a variation of engine speed. The researcher presented the vibration that occurred in a 2D graphical representation and the Z-freq coefficient showed an increase in value as the misfire happened inside the gasoline engine. This paper aims to evaluate the rotor unbalance fault based on Z-freq coefficient. Three faults were created using the machine simulator: static, couple, and dynamic. Z-freq coefficient would give significant results as an alternative method in determining the rotor unbalance due to faulty.

2. Methodology

2.1 Z-Freq Statistical Method

The Z-freq statistical method was developed by transferring the collected data to the frequency domain using Fast Fourier Transform (FFT). The randomly collected data is further classified into moments r-th order of discrete signal in the frequency band, which the formula as per below.

$$M_r = \frac{1}{N} \sum_{i=1}^{n} \left(f_i \right) \qquad (1)$$

Where N is the number of data, r is the order of the moment, f_i is i-th frequency and $\overline{f}$ is an average frequency.

Kurtosis, which is the signal 4th statistical moment, is a global signal statistic that is highly sensitive to the spikiness of the data. For a Gaussian distribution, the kurtosis value is roughly 3.0. Higher kurtosis values indicated the presence of extreme values in a Gaussian distribution. Kurtosis analysis was utilized to identify fault symptoms because of its sensitivity to large magnitude.

The kurtosis value is defined by:

$$K = \frac{1}{n\sigma^4} \sum_{i=1}^{n} \left(f_i - \overline{f} \right)^4 \qquad (2)$$

Where, σ is the standard deviation, and K is the Kurtosis value. Based on this, the Z-freq approach generates a 2-D graphical representation of its coefficient result. The frequency domain signal was split into two frequency groups: the x-axis representing low frequency (affix) and the y-axis representing high frequency (annex). Affix mob is made up of frequency mobs ranging from 0.5fmax to 1.0fmax.

Z-freq calculates the data distance to the signal centroid, as shown in the equation below.

The Z-freq coefficient is defined by:

$$Z^f = \frac{1}{n} \sqrt{K_{afx} s_{afx}^4 + K_{anx} s_{anx}^4} \qquad (3)$$

where K_{afx} is kurtosis and s_{afx} is the standard deviation for the low-frequency range and K_{anx} is kurtosis and s_{anx} is the standard deviation for the high-frequency range.

2.2 Experimental Setup

The experiment was set up using the fault simulator machine brand Spectra Quest. Two 6" aluminum rotor disks were attached with the 3 phase 1 HP electric motor to stimulate unbalance of the rotor. The disk has 36 threaded holes at 10-degree intervals and then was inserted with a screw for three types of faults as in Fig. 1. At the same time, the steel rotor shaft with ¾" diameter was given a load of 10Nm at the other end. Then it was then attached with Phantom Universal Accelerometer Wireless Adapter (GP8) and Phantom Gateway was setup as per Fig. 2. The GP8 will wirelessly connected to Phantom Gateway. Then the Phantom Gateway will be connected to the Wi-Fi, transferring all the data to a laptop for further analysis. Each data set was run three times for five different speeds: 400 RPM, 800 RPM, 1200 RPM, 1600 RPM and 2000 RPM. The fault signal monitoring activity is illustrated in the flowchart as shown in Fig. 3. The signal data was then divided into two frequency bands, affix (low frequency) and annex (high frequency). The annex frequency band refers to the frequency between half of the maximum frequency and the maximum frequency range. In contrast, affix frequency refers to the frequency between half of the maximum and minimum frequency ranges. The activity continues with calculating kurtosis values and standard deviation for each signal. The derivation of Z-freq coefficient for each fault and speed was then calculated. A classification based on machine learning was applied to differentiate each rotor speed. Then, the correlation between signal and fault was examined. The training will be repeated until satisfactory results are obtained during verification. Finally, using simulation software, the Z-freq value's scattering was represented in a 2-D graphical scattering plot.
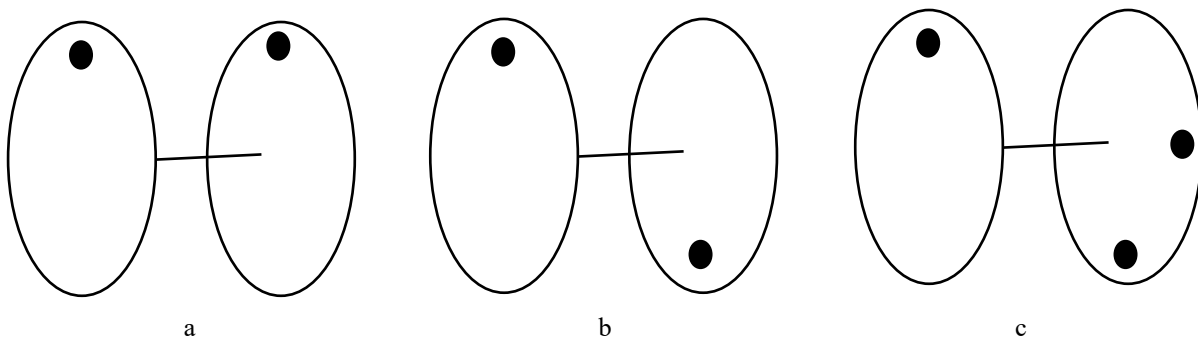

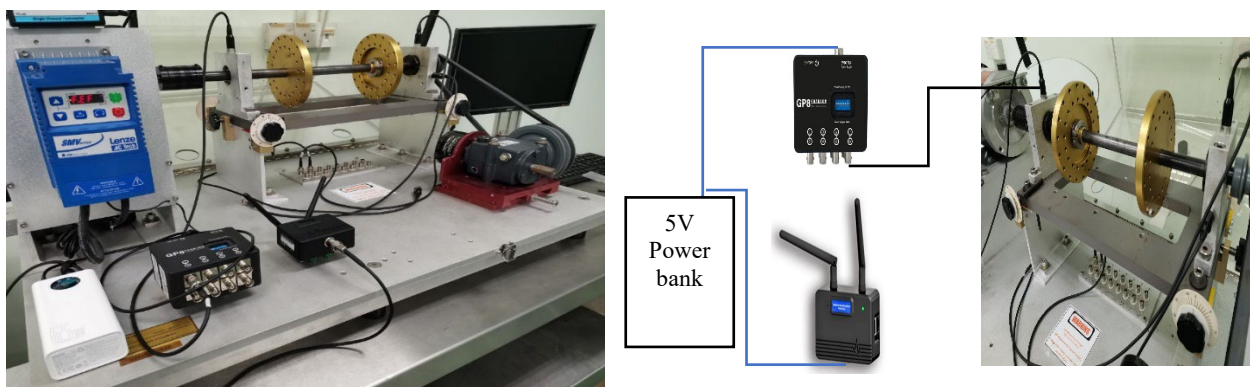Fig. 1 - Unbalance faulty types (a) static; (b) coupled; (c) dynamic

Fig. 2 - Experimental setup diagram

3. Result and Discussion

In this section, all findings are graphically well presented and in coefficient value to be easier to interpret. The result will discuss the finding of all rotor speeds and all rotor conditions to check whether the proposed technique can be applied significantly in that specific application. During the measurement, five different speeds were acquired: 400RPM, 800RPM, 1200RPM, 1600RPM and 2000RPM. Faults set up are Normal condition, Static unbalance condition, Coupled unbalance condition and Dynamic unbalance condition. Fig. 4 displays the vibration result in an acceleration unit of the rotor under normal conditions for two speeds (a) 400RPM and (b) 2000RPM. For a low-speed rotor, the vibration acceleration shows a low value in the time and frequency domains. It proves that the rotor is still in good condition and more stable. For high-speed rotation, the time and frequency domain value increased approximately

four times compared to low speed. This can be summarized that the vibration of the rotor significantly increased with speed and became unstable but acceptable.

```
                              ┌─────────┐
                              │  Start  │
                              └─────────┘
         ┌────────────────────────┼────────────────────────┐
         ▼                        │                        ▼
 ┌─────────────────┐              │              ┌─────────────────┐
 │   Static Fault  │              │              │  Dynamic Fault  │
 └─────────────────┘              │              └─────────────────┘
         └────────────────────────┼────────────────────────┘
                                  ▼
                  ╱───────────────────────────────╲
                  │ Rotor Vibration Signal Measurement │
                  ╲───────────────────────────────╱
                                  ▼
                  ┌───────────────────────────────┐
                  │     Noise Signal Filtering     │
                  └───────────────────────────────┘
                                  ▼
                  ┌───────────────────────────────┐
                  │ Decomposition of data into 2 frequency mobs │
                  └───────────────────────────────┘
              ┌───────────────────┴───────────────────┐
              ▼                                         ▼
  ┌───────────────────────┐              ┌───────────────────────────┐
  │  Affix: 0-0.5f_max     │              │  Annex: 0.5f_max - f_max  │
  └───────────────────────┘              └───────────────────────────┘
              ▼                                         ▼
  ┌───────────────────────┐              ┌───────────────────────────┐
  │ Calculation of K_1 & s_1 │            │ Calculation of K_2 & s_2 │
  └───────────────────────┘              └───────────────────────────┘
              └───────────────────┬───────────────────┘
                                  ▼
                  ┌───────────────────────────────┐
                  │ Calculation of Z-freq Coefficient │
                  └───────────────────────────────┘
                                  ▼
                  ┌───────────────────────────────┐
                  │     Signal Classification      │◄──────┐
                  └───────────────────────────────┘       │
                                  ▼                         │
                  ┌───────────────────────────────┐       │
                  │ Correlation between signal and faults │  │
                  └───────────────────────────────┘       │
                                  ▼                         │
                         ◇───────────────◇    N            │
                         │  Verification  │────────────────┘
                         ◇───────────────◇
                                  │ Y
                                  ▼
                  ╱───────────────────────────────╲
                  │  2D Representation of Z-freq   │
                  ╲───────────────────────────────╱
                                  ▼
                              ┌─────────┐
                              │  Stop   │
                              └─────────┘
```
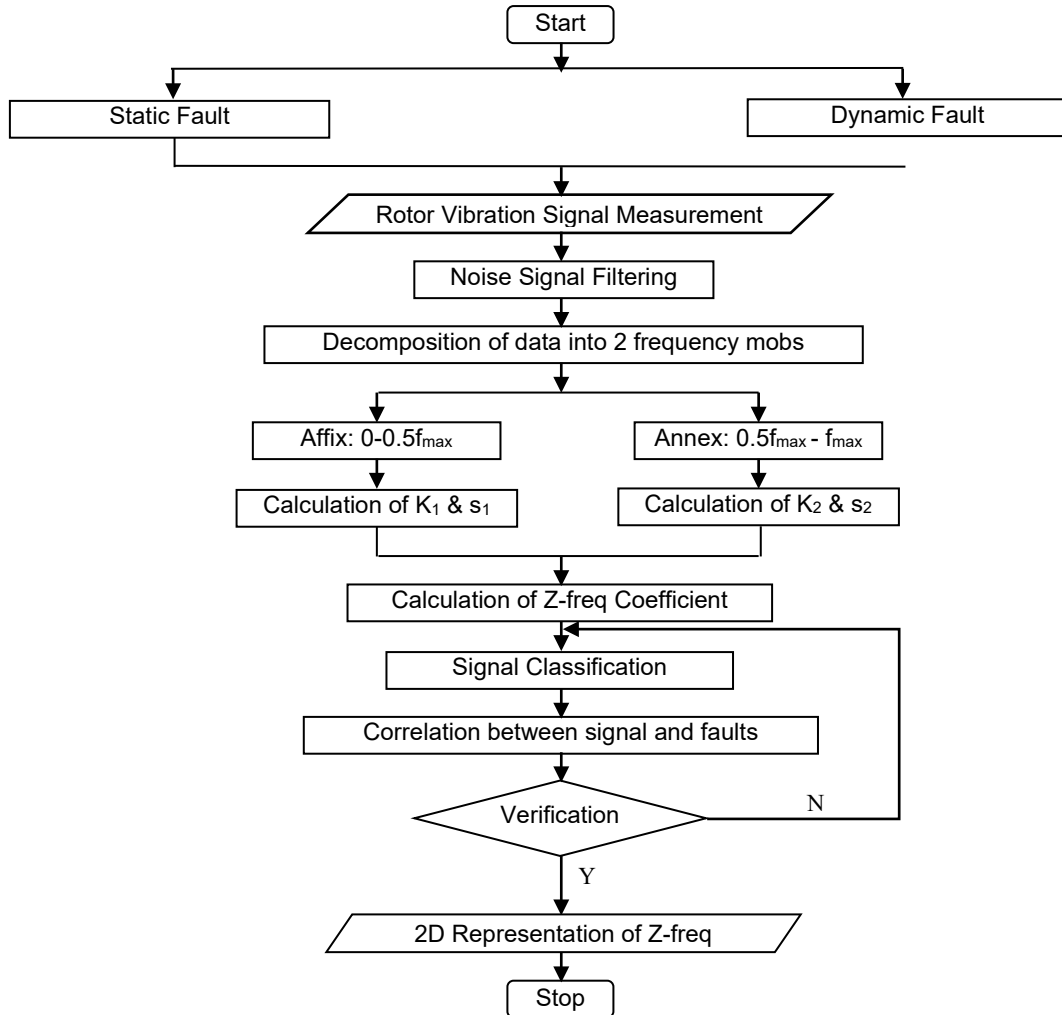
Fig. 3 - Rotor disk faults diagnostic process flow using Z-freq

Fig. 5 provides the scattering of I-kaz and Z-freq coefficient values for rotor rotates in average conditions. This representation also covers two speeds: low speed at 400RPM and high speed at 2000RPM. As presented in the graph, I-kaz representation becomes scattered as the speed increases, proving this method can differentiate the rotor's speed. To distinguish using the Z-freq technique, three colors representation also depicts the pattern of speed increment. A closer inspection of the graph shows that the red color scattering representation is wider than the other two colors. It concludes that pair of affix and annex frequencies can detect the speed pattern. The Z-freq distribution uses a color-coding scheme to depict the range of frequencies in the frequency domain. Low-frequency pairs are represented by green, medium-frequency by yellow, and high-frequency by red. The color-coding scheme is based on the following ranges: Low-frequency pairs: affix frequency 1 to 400 Hz and annex frequency 1201 to 1600 Hz, Medium-frequency pairs: affix frequency 401 to 600 Hz and annex frequency 1001 to 1200 Hz, High-frequency pairs: affix frequency 601 to 800 Hz and annex frequency 801 to 1000 Hz. Each axis (horizontal and vertical) in the figure shows the number of frequency pairs that fall within the range for that axis. The color-coding scheme allows for quick and easy visualization of the distribution of frequencies in the frequency domain. Three figures from Fig. 6 shows the plot of coefficient values of Z-freq, I-kaz and RMS for Normal condition. From these graphs, all patterns of speed increment are the same and clear. The coefficient of determination (R^2) is also at an acceptable level of more than 90%. The most exciting aspect of these graphs is that all techniques are valid for detecting and predicting vibration signals generated over rotor speeds.
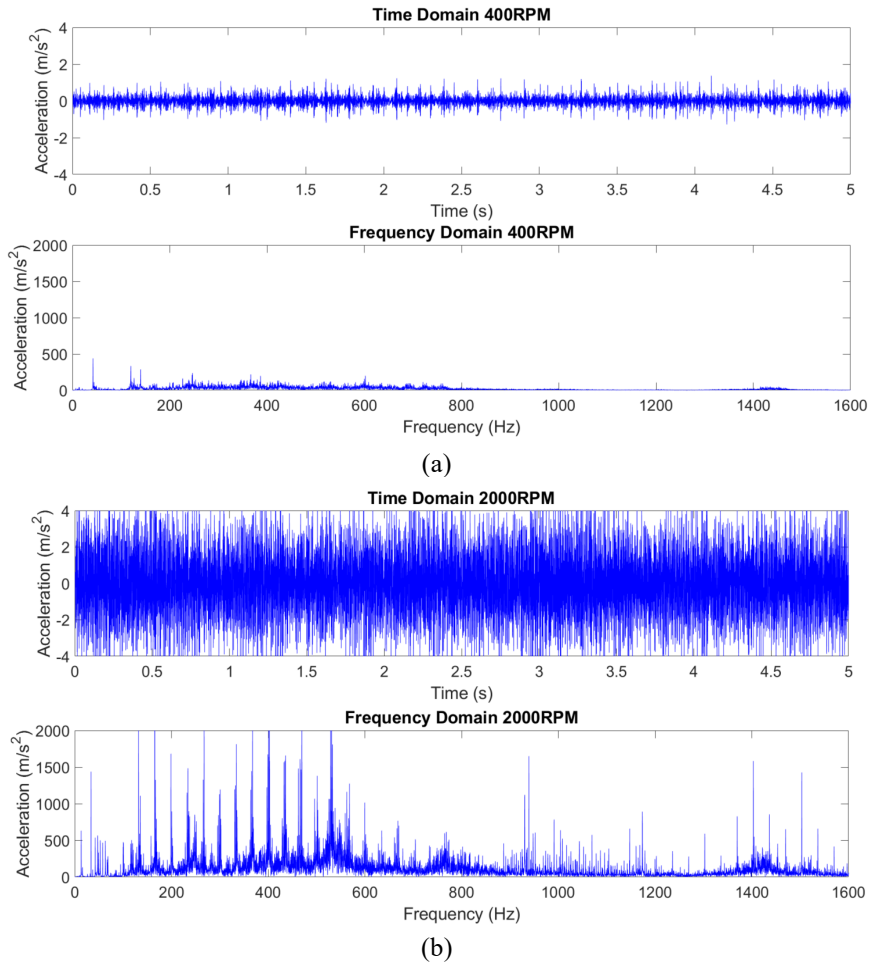
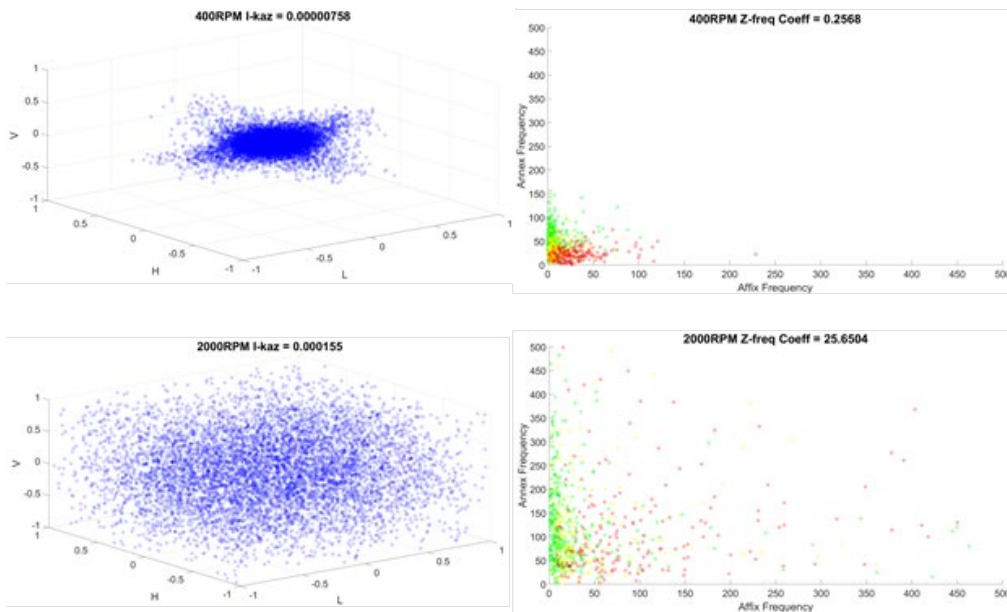**Fig. 4 - Time and frequency domain for rotor equipment at 400RPM and 2000RPM**

Fig. 5 - I-kaz and Z-freq representation for rotor equipment at 400RPM and 2000RPM
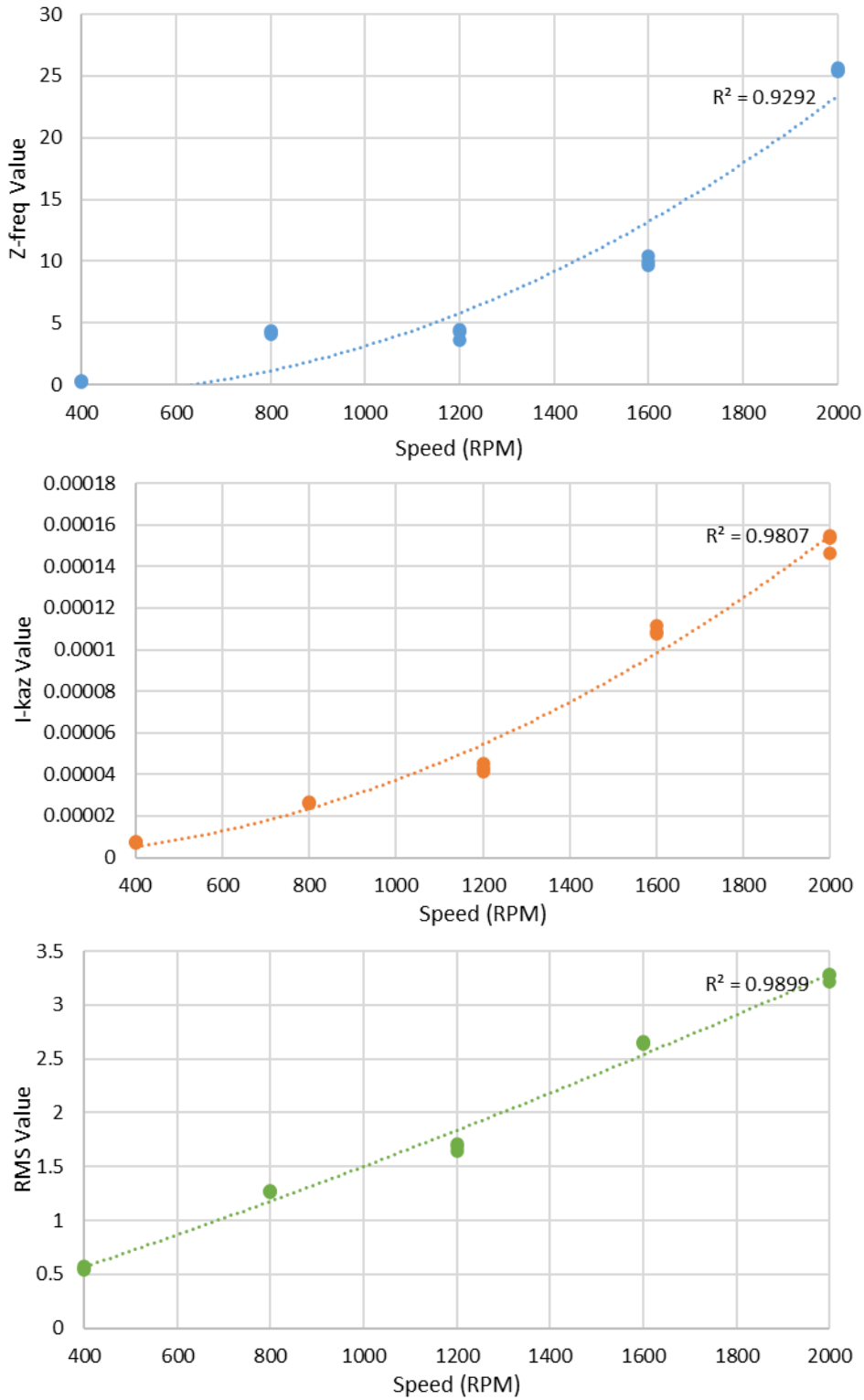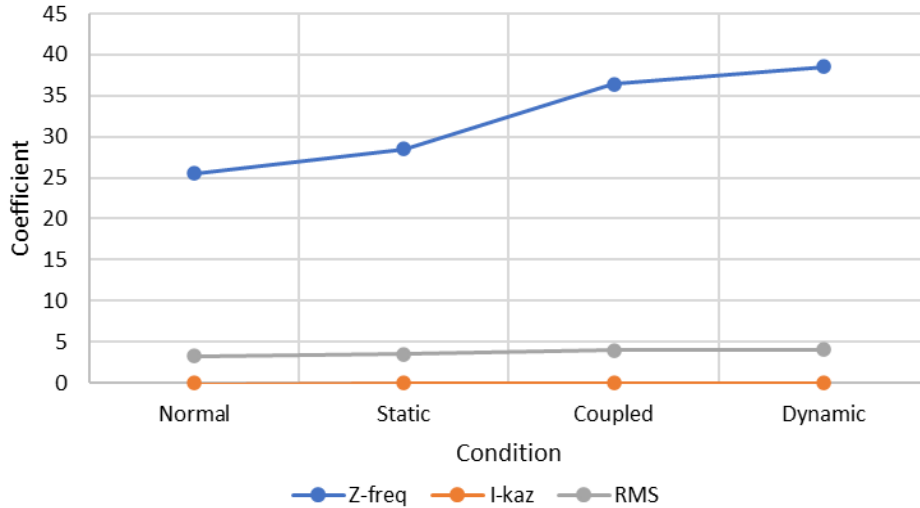
Fig. 6 - Z-freq, I-kaz and RMS at normal condition for rotor equipment with speed (RPM) 400, 800, 1200, 1600 and 2000

Fig. 7 - I-kaz and Z-freq representation for rotor faults (normal, static, coupled, and dynamic) at 400RPM and 2000RPM

Fig. 7 was plotted from Table 1. As Fig. 7 shows, there is a summary of Z-freq, I-kaz and RMS coefficient values for all speeds calculated and a significant conclusion was obtained. This study proved that a hypothesis of Z-freq and the other two techniques could find patterns of data measured. A strong relationship between the speed of the rotor and the coefficient value. The results of a signal analysis conducted on the rotor at various velocities are presented in Table 1. The Z-freq, I-kaz, and RMS values for each speed provide insightful information regarding the mechanical behavior of the rotor instability system. Z-freq increases with increasing speed, indicating that the mechanical characteristics of the rotor unbalance system change at higher RPMs. Similarly, I-kaz and RMS values exhibit an upward trend with increasing system speed, indicating changes in vibration or mechanical response.

It can be seen from Table 2, all three types of analysis techniques challenge it capability to detect and predict symptoms of rotor fault, such as static unbalance, coupled unbalance, dynamic unbalance and normal condition. From the tabulated data, an initial objective has been met, which this new method named Z-freq can differentiate the fault pattern. [12], [13] From this observation, there is a little increment for static fault, about 12% from the normal condition for Z-freq value, a significant increment of about 43% for coupled fault and 51% for dynamic fault. This little percentage difference between coupled and dynamic also occurred in I-kaz and RMS.

Table 1 - Summary of Z-freq, I-kaz and RMS coefficient for all speeds

Speed	Z-freq	I-kaz	RMS
400	0.2568	0.0000074	0.5572
800	3.5946	0.0000261	1.2678
1200	4.3321	0.0000429	1.6874
1600	10.4388	0.0001090	2.6504
2000	25.4989	0.0001540	3.2798

Table 2 - Summary of Z-freq, I-kaz and RMS coefficient for all conditions at 2000RPM

Condition	Z-freq	I-kaz	RMS
Normal	25.4989	0.0001540	3.2798
Static Fault	28.4721	0.000176	3.4808
Coupled Fault	36.4186	0.000234	3.9402
Dynamic Fault	38.5483	0.000240	4.0453

4. Conclusion

This investigation aimed to diagnose a rotor unbalance fault under five different speeds with the application of load torque. This goal has been achieved through the result presented in the previous section. The study set out a prediction for fault diagnosis with a high coefficient of determination. A successfully strong correlation of every condition investigated has been found and can be helpful for future troubleshooting. One of the more significant findings to emerge from this study is that wireless monitoring could be the future of vibration analysis and monitoring of mechanical machines, which is a potential hazard that can be avoided.

Acknowledgement

References

[1] M. Jreige, M. Abou-Zeid, and I. Kaysi, "Consumer preferences for hybrid and electric vehicles and deployment of the charging infrastructure: A case study of Lebanon," *Case Stud. Transp. Policy*, vol. 9, no. 2, pp. 466-476, 2021, doi: 10.1016/j.cstp.2021.02.002.

[2] Y. Qin *et al.*, "Noise and vibration suppression in hybrid electric vehicles: State of the art and challenges," *Renew. Sustain. Energy Rev.*, vol. 124, no. February, p. 109782, 2020, doi: 10.1016/j.rser.2020.109782.

[3] N. Wang and D. Jiang, "Vibration response characteristics of a dual-rotor with unbalance-misalignment coupling faults: Theoretical analysis and experimental study," *Mech. Mach. Theory*, vol. 125, pp. 207-219, 2018, doi: 10.1016/j.mechmachtheory.2018.03.009.

[4] P. Wang, H. Xu, Y. Yang, H. Ma, D. He, and X. Zhao, "Dynamic characteristics of ball bearing-coupling-rotor system with angular misalignment fault," *Nonlinear Dyn.*, vol. 108, no. 4, pp. 3391-3415, 2022, doi: 10.1007/s11071-022-07451-1.

[5] H. Cao, D. He, S. Xi, and X. Chen, "Vibration signal correction of unbalanced rotor due to angular speed fluctuation," *Mech. Syst. Signal Process.*, vol. 107, pp. 202-220, 2018, doi: 10.1016/j.ymssp.2018.01.030.

[6] Z. Jian *et al.*, "Online unbalance compensation of a maglev rotor with two active magnetic bearings based on the LMS algorithm and the influence coefficient method," *Mech. Syst. Signal Process.*, vol. 166, no. October 2021, p. 108460, 2022, doi: 10.1016/j.ymssp.2021.108460.

[7] R. Ambur and S. Rinderknecht, "Unbalance detection in rotor systems with active bearings using self-sensing piezoelectric actuators," *Mech. Syst. Signal Process.*, vol. 102, pp. 72-86, 2018, doi: 10.1016/j.ymssp.2017.09.006.

[8] C. Mongia, D. Goyal, and S. Sehgal, "Vibration response-based condition monitoring and fault diagnosis of rotary machinery," *Mater. Today Proc.*, vol. 50, pp. 679-683, 2022, doi: 10.1016/j.matpr.2021.04.395.

[9] L. Lan, X. Liu, and Q. Wang, "Fault detection and classification of the rotor unbalance based on dynamics features and support vector machine," *Meas. Control (United Kingdom)*, vol. 56, no. 5-6, pp. 1075-1086, 2023, doi: 10.1177/00202940221135917.

[10] C. L. Lin, J. W. Liang, Y. M. Huang, and S. C. Huang, "A novel model-based unbalance monitoring and prognostics for rotor-bearing systems," *Adv. Mech. Eng.*, vol. 15, no. 1, pp. 1-16, 2023, doi: 10.1177/16878132221148019.

[11] M. A. F. Ahmad, M. Z. Nuawi, J. A. Ghani, S. Abdullah, and A. N. Kasim, "Tool wear monitoring using macro fibre composite as a vibration sensor via I-kaz^{TM} statistical signal analysis," *ARPN J. Eng. Appl. Sci.*, vol. 13, no. 11, pp. 3607-3616, 2018.

[12] N. A. Ngatiman, M. Z. Nuawi, and S. Abdullah, "Z-freq: Signal analysis-based gasoline engine monitoring technique using piezo-film sensor," *Int. J. Mech. Eng. Technol.*, vol. 9, no. 5, pp. 897-910, 2018.

[13] N. A. Ngatiman, M. Z. Nuawi, A. Putra, I. S. Qamber, T. Sutikno, and M. H. Jopri, "Spark plug failure detection using Z-freq and machine learning," *Telkomnika (Telecommunication Comput. Electron. Control.*, vol. 19, no. 6, pp. 2020-2029, 2021, doi: 10.12928/TELKOMNIKA.v19i6.22027.